Early Results from GLASS-JWST XXII: Rest frame UV-optical spectral properties of Lyman-alpha emitting galaxies at 3 < z < 6

NAMRATA ROY,[1] ALAINA HENRY,[2, 1] TOMMASO TREU,[3] TUCKER JONES,[4] GONZALO PRIETO-LYON,[5, 6] CHARLOTTE MASON,[5, 6] TIM HECKMAN,[1] THEMIYA NANAYAKKARA,[7] LAURA PENTERICCI,[8] SARA MASCIA,[8] MARUŠA BRADAČ,[9, 4] EROS VANZELLA,[10] CLAUDIA SCARLATA,[11] KIT BOYETT,[12, 13] MICHELE TRENTI,[12, 13] AND XIN WANG[14, 15, 16]

[1]Center for Astrophysical Sciences, Department of Physics and Astronomy, Johns Hopkins University, Baltimore, MD, 21218
[2]Space Telescope Science Institute, 3700 San Martin Drive, Baltimore MD, 21218
[3]Department of Physics and Astronomy, University of California, Los Angeles, 430 Portola Plaza, Los Angeles, CA 90095, USA
[4]Department of Physics and Astronomy, University of California Davis, 1 Shields Avenue, Davis, CA 95616, USA
[5]Cosmic Dawn Center (DAWN), Denmark
[6]Niels Bohr Institute, University of Copenhagen, Jagtvej 128, DK-2200 Copenhagen N, Denmark
[7]Centre for Astrophysics and Supercomputing, Swinburne University of Technology, PO Box 218, Hawthorn, VIC 3122, Australia
[8]INAF - Osservatorio Astronomico di Roma, via di Frascati 33, 00078 Monte Porzio Catone, Italy
[9]University of Ljubljana, Department of Mathematics and Physics, Jadranska ulica 19, SI-1000 Ljubljana, Slovenia
[10]INAF – OAS, Osservatorio di Astrofisica e Scienza dello Spazio di Bologna, via Gobetti 93/3, I-40129 Bologna, Italy
[11]School of Physics and Astronomy, University of Minnesota, Minneapolis, MN, 55455, USA
[12]School of Physics, University of Melbourne, Parkville 3010, VIC, Australia
[13]ARC Centre of Excellence for All Sky Astrophysics in 3 Dimensions (ASTRO 3D), Australia
[14]School of Astronomy and Space Science, University of Chinese Academy of Sciences (UCAS), Beijing 100049, China
[15]National Astronomical Observatories, Chinese Academy of Sciences, Beijing 100101, China
[16]Institute for Frontiers in Astronomy and Astrophysics, Beijing Normal University, Beijing 102206, China

ABSTRACT

Lyα emission is possibly the best indirect diagnostic of Lyman continuum (LyC) escape since the conditions that favor the escape of Lyα photons are often the same that allows for the escape of LyC photons. In this work, we present the rest UV-optical spectral characteristics of 11 Lyα emitting galaxies at $3 < z < 6$ - the optimal redshift range chosen to avoid the extreme IGM attenuation while simultaneously studying galaxies close enough to the epoch of reionization. From a combined analysis of JWST/NIRSpec and MUSE data, we present the Lyα escape fraction and study their correlations with other physical properties of galaxies that might facilitate Lyα escape. We find that our galaxies have low masses (80% of the sample with $\log_{10} M_\star < 9.5 M_\odot$), compact sizes (median $R_e \sim 0.7$ kpc), low dust content, moderate [OIII]/[OII] flux ratios (mean $\sim 6.8 \pm 1.2$), and moderate Lyα escape fraction (mean $f_{esc}^{Ly\alpha} \sim 0.11$). Our sample show characteristics that are broadly consistent with the low redshift galaxies with Lyα emission, which are termed as "analogs" of high redshift population. We predict the Lyman continuum escape fraction in our sample to be low (0.03-0.07), although larger samples in the post-reionization epoch are needed to confirm these trends.

Keywords: Galaxies: emission lines – Galaxies: high-redshift – Galaxies: evolution

1. INTRODUCTION

One of the main science drivers behind the James Webb Space Telescope (JWST) is spectroscopic confirmation and characterization of the galaxies formed during the crucial epoch of Cosmic Reionization (EoR), i.e., when the inter-galactic medium (IGM) transforms from neutral to completely ionized state (see Robertson 2022, for a review). The Lyman-continuum (LyC, $\lambda < 912$ Å) photons escaping into the neutral IGM from the star-forming galaxies can reionize the Universe by z = 6 only if a substantial fraction ($\sim$ 10 %) of the photons escape from the galaxies' interstellar and circumgalactic media (ISM and CGM; e.g., Finkelstein et al. 2019; Robertson et al. 2015). Early data from JWST has revealed insights into the ISM conditions and ion-

Corresponding author: Namrata Roy
nroy13@jhu.edu

izing photon production in reionization-era galaxies at z > 6 (Curtis-Lake et al. 2022; Robertson et al. 2022; Cameron et al. 2023; Trump et al. 2023; Tacchella et al. 2022; Fujimoto et al. 2023). However, directly estimating the escape fraction of the LyC photons (f_{esc}) is almost impossible at z > 4.5 since the photons get absorbed by the dense neutral IGM along the line of sight (Inoue et al. 2014).

While a number of indirect tracers have been used to predict LyC f_{esc}– e.g., [SII] emission deficit, Mg II emission, high [OIII]/[OII] emission (Zackrisson et al. 2013; Nakajima & Ouchi 2014; Wang et al. 2021; Katz et al. 2022; Flury et al. 2022), one of the best indicators of LyC f_{esc} is the Lyα emission – the brightest nebular recombination line of hydrogen atom (e.g., Pahl et al. 2021; Gazagnes et al. 2020). LyC leakers tend to show strong Lyα emission escape (Nakajima et al. 2020). Since Lyα scatters resonantly in H I, the resultant emission profile bears information about the neutral hydrogen in the IGM and the epoch of reionization (Stark et al. 2010; Treu et al. 2012), as well as the gas covering fraction, column density, and dust geometry of the host galaxy from which the intrinsic Lyα emission emerges (Neufeld 1991). Since Lyα remains the strongest diagnostic and has now been observed in some of the highest redshift galaxies using JWST (Saxena et al. 2023; Bunker et al. 2023; Boyett et al. 2023; Mascia et al. 2023), it is now essential to understand the physical processes that determine Lyα escape, and to disentangle the effects of the ISM and IGM.

Over the last several years, studies have aimed to understand the escape of Lyα emission from galaxies at redshifts where the IGM is fully ionized. With the union of HST/ Cosmic Origins Spectrograph (COS) and the SDSS, samples of low-redshift ($z \lesssim 0.5$) analog galaxies have been studied with detailed spectroscopic coverage from the rest-frame UV to optical (blueberries, green peas, Lyman break analogs, Lyman continuum emitters; Cardamone et al. 2009; Heckman et al. 2011, 2015; Yang et al. 2017b,a; Henry et al. 2015; Jaskot & Oey 2013; Hayes et al. 2023; Flury et al. 2022). Diagnostics to predict Lyα properties have begun to emerge: Hayes et al. (2013, 2014) show how the spatial extent of the scattered Lyα emission varies with galaxy properties. Other studies investigate the escape fraction of Lyα photons and the galaxy characteristics that promote strong Lyα emission (Henry et al. 2015; Rivera-Thorsen et al. 2015; Yang et al. 2017b). Moreover, Mg II emission has been shown to correlate strongly with Lyα, further indicating low column densities in the ISM (Henry et al. 2018; Chisholm et al. 2020; Xu et al. 2022, 2023). And, importantly, low-redshift analogs have been used to develop predictors for LyC escape (Heckman et al. 2011; Izotov et al. 2016, 2018; Flury et al. 2022), demonstrating the strong link between LyC and Lyα.

However, a critical question remains: *are these diagnostics and correlations applicable in the reionization epoch?*

The answer to this question bears heavily on our interpretation of the high-redshift galaxy samples now being uncovered with JWST. An initial spectroscopic census of JWST galaxies above z > 7 seems to indicate elevated ionization parameters, low metallicities, low dust content, high specific star formation rates (sSFR), and higher ionizing radiation escape fraction than seen locally (Katz et al. 2023; Curti et al. 2023; Cameron et al. 2023; Sanders et al. 2023). While many of these galaxies resemble the extreme ISM conditions observed in low-redshift analogs, we cannot be certain if the similarities extend to Lyα and LyC. Therefore, the critical next step is to verify our low-z diagnostics in the post-reionization epoch. JWST's access to the rest-frame optical spectra of galaxies at z$\sim$ 3 − 6 now provides the complete spectroscopic coverage needed to make this possible.

In this paper, we focus on Lyα. Since nearly all low-z analog galaxies show strong Lyα emission, their most obvious counterparts at $z > 3$ are Lyα-selected galaxies. Therefore, we present a rest frame UV-optical spectroscopic study of 11 Lyα emitting galaxies (LAEs) at 3<z < 6, selected using the Multi-Unit Spectroscopic Explorer (MUSE) instrument at the ESO-VLT. The redshift range is optimally chosen to include moderate to high redshift galaxies, not exceeding beyond z > 6.5, where Lyα emission gets significantly attenuated due to the IGM (Pentericci et al. 2018; Fuller et al. 2020). We utilize the JWST/NIRSpec spectra obtained in the Abell 2744 cluster field as part of the JWST Early Release Science program GLASS (Treu et al. 2022) to confirm spectroscopic redshifts and measure rest frame optical line ratios and EWs with high precision. We look for the possible evolution of the Lyα output of galaxies by comparing to low-z analogs galaxies observed with COS. Although our sample of 11 sources is not large, our objects provide a critical benchmark for future comparisons as more and more JWST data become available over the coming years.

In §2, we describe the observations used in this study and the chosen sample. In §3, we describe the analysis methods and measurements of the rest frame UV-optical spectral properties that we use throughout this work. In §4 & 5, we present the main results. In §6, we discuss the implications of the result and end with a conclusion in §7.

2. DATA ACQUISITION AND SAMPLE DEFINITIONS

This work focuses on 11 Lyα emitting sources in the field of the lensing cluster Abell 2744. Our study uses spatially resolved optical IFU spectroscopic data from VLT/MUSE and deep near-infrared spectroscopy from JWST/NIRSpec to obtain rest frame UV-optical spectra. The final list of targets in our sample and their properties are listed in Table 1, and the details of the sample selection are discussed in the sections to follow.

2.1. *VLT/MUSE spectroscopy*

Optical spectroscopy using the VLT/MUSE instrument was performed on the Abell 2744 cluster region as part of the GTO program 094.A-0115 (PI: Richard; Mahler et al. 2018; Richard et al. 2021). The program targeted the central regions of the massive cluster using the wide field mode, with a 2 arcmin × 2 arcmin mosaic of MUSE pointings. The wavelength coverage of the observations ranges between 4750 to 9350 Å, with a spectral resolution varying between R = 2000 - 4000. The reduced datacubes are publicly available in the form of fits files[1]. Mahler et al. (2018) published the full spectroscopic catalog of objects with measured redshifts. Richard et al. (2021) published a follow-up catalog of Lyα emission line measurements, with an emission line detection limit of $(0.77-1.5) \times 10-18$ erg s^{-1} cm^{-2} at 5σ. This parent catalog of MUSE LAEs was used to select a subset of 17 LAEs that were observed with NIRSpec as part of the GLASS-JWST program.

2.2. *JWST/NIRSpec spectroscopy*

This work uses near-infrared spectroscopic data in the Abell 2744 field obtained from the GLASS-JWST Early Release Science (ERS) program (ID 1324, PI Treu; Treu et al. 2022). This observation provides high-resolution spectroscopy (R = 2700) over an observed wavelength range of $\lambda_{obs} \sim 0.8$ - 5.2 μm using the NIRSpec multi-object spectroscopy mode. The GLASS-JWST observations were carried out with three spectral configurations: G140H/F100LP (0.97 - 1.82 μm), G235H/F170LP (1.66 - 3.05μm) and G395H/F290LP (2.87 - 5.14 μm). Each of the three high-resolution gratings was exposed for 4.9 hours. The MSA target selection is discussed in Treu et al. (2022). All the *JWST* data used in this paper can be found in MAST: 10.17909/fqaq-p393.

We use the official STScI JWST pipeline[2] (version 1.8.2) and the msaexp code[3] with the updated set of reference files that include in-flight flux calibrations (CRDS_CONTEXT = "jwst_1041.pmap") to produce Level 2 and 3 products. Morishita et al. (2022) have discussed the data reduction process and observation strategy in detail. In short, we downloaded the Level 1b data products from the MAST portal[4]. calwebb_detector1, which is the first step of the reduction, was already run on the raw detector exposures and are provided in the Level 1b outputs. We implement the second and third steps of the reduction: calwebb_spec2 and calwebb_spec3 routines to perform flat-fielding, wave-

length calibrations, path-loss corrections, and background subtractions. Nodded observations of our MSA slitlet exposures were used to perform local background subtraction since our sources are compact. The resultant 2D spectra are visually inspected, and the 1D spectra are optimally extracted, following the method outlined by Horne (1986).

The high spectral resolution and the broad wavelength coverage of NIRSpec enable detection of the standard rest-frame optical emission lines like [OII]$\lambda\lambda$3727, 3729 Å, Hβ, [OIII]$\lambda\lambda$4959, 5007 Å, and Hα up to $z \sim 7$, allowing for precise measurements of optical spectral properties of our sources.

2.3. *Sample selection*

A sample of 17 MUSE LAEs with confident Lyα redshifts were included in the NIRSpec MSA configuration. This sample is not magnitude complete but provides an ideal sample to compare with the nearby UV-bright green pea population (Henry et al. 2015; Yang et al. 2017b), extreme emission line galaxies (Erb et al. 2016), Lyman Break Analogs (Heckman et al. 2015), Lyman continuum leaking galaxies (Izotov et al. 2016) and starbursts (Rivera-Thorsen et al. 2015, 2017) in the literature, which are believed to be low redshift analogs of high-z LAEs. 12 of those 17 LAEs show strong rest frame optical line detection whose redshifts and spectral properties can be measured with confidence (Mascia et al. 2023), Prieto-Lyon et al. 2023 (in prep). One of these 12 shows very faint Lyα detection with insufficient S/N below 3. We use the remaining 11 LAEs as the core sample for this work (Table 1). Our sample is identical to Prieto-Lyon et al. 2023 (in prep), who focus on the Lyα velocity offsets.

2.4. *Catalogs*

We use the redshifts from Mahler et al. (2018) catalog to primarily select our 11 Lyα emitting galaxies at z > 3. The catalog is publicly available [5]. We used the UV-rest frame continuum measurements from Richard et al. (2021) catalog in our analyses. The UV continuum is derived using the photometric catalogs for Abell 2744, which includes photometry information from the HST/ACS and WFC3/IR of the Hubble Frontier Fields project (HST-GO/DD-13495; Lotz et al. 2017). We use the ASTRODEEP catalog [6] from Merlin et al. (2016), and Castellano et al. (2016) for reporting the stellar mass and star formation rates of our targets. The stellar 238 mass and star formation rate estimates are derived from SED 239 fitting, taking into account the nebular emission line contribution. See Castellano et al. (2016) for details.

2.5. *Comparison Sample*

[1] http://muse-vlt.eu/science/a2744

[2] https://github.com/spacetelescope/jwst

[3] https://github.com/gbrammer/msaexp

[4] https://mast.stsci.edu/portal/Mashup/Clients/Mast/Portal.html

[5] http://data.muse-vlt.eu/A2744/A2744_redshifts_cat_final.txt

[6] http://www.astrodeep.eu/frontier-fields/

We aim to test whether the low redshift ($z \lesssim 0.4$) analogs of high-z LAEs are similar to the LAEs at a cosmologically significant redshift (z> 3) in terms of rest frame optical spectral properties. But first, we place our high z sample in the context of the broader z∼ 3-6 LAE population previously reported in the literature. To select an emission line survey for z = 3-6 LAEs to be compared with our sample, we use the publicly available MUSE observations taken in the Hubble Ultra Deep Field (HUDF) region (Bacon et al. 2023; Inami et al. 2017). We chose this survey since this is the deepest spectroscopic survey ever performed, and the catalog contains the most comprehensive measurements we require to compare with our high redshift sources. The catalog is available through the CDS/ Vizier database or the MUSE data products website [7].

For the low redshift analog population, we use Hayes et al. (2023) as our primary sample, which compiles the HST/COS observations of 87 UV-bright galaxies. The COS data are drawn from: GO 11522 (PI: Green), 11727 (Heckman), 12027 (Green), 12269 (Scarlata), 12583 (Hayes), 12928 (Henry), 13017 (Heckman), 13293 (Jaskot), 13744 (Thuan), 14080 (Jaskot), 14201 (Malhotra), 14635 (Izotov), 15136 (Izotov), 15639 (PI: Izotov), and 15865 (PI: Henry). This comprehensive sample includes sources that are frequently classified as low-redshift analogs of high-z galaxies due to their strong Lyα emission and emission line properties - like the Green pea population, Lyman continuum leaking galaxies, extreme emission line galaxies, Lyman break analogs, and compact starbursts (Heckman et al. 2011, 2015; Wofford et al. 2013; Henry et al. 2015; Rivera-Thorsen et al. 2015, 2017; Izotov et al. 2016, 2018; Jaskot et al. 2017, 2019; Yang et al. 2017b; Izotov et al. 2021; Xu et al. 2022). The corresponding rest-optical data are obtained from the Sloan Digital Sky Survey (SDSS) Data Release 16 (DR16; Ahumada et al. 2020). The Lyα and optical emission line properties measurements for this extensive sample are obtained from Hayes et al. (2023) via private communication. These galaxies are in the redshift range between z = 0.020 and z = 0.44 and sample a large range in stellar mass and star formation rates. We refer to this compilation of galaxies as low-z analogs. In addition to the sample described above, we include 88 Lyman continuum emitter candidates from the low z Lyman continuum survey (LzLCs) sample (Flury et al. 2022). 50% of these galaxies are confirmed LyC leakers. All galaxies in this sample exhibit strong Lyα emission.

3. DATA ANALYSES AND MEASUREMENTS

We construct Lyα narrowband images (NB) from the MUSE data, following Leclercq et al. (2017), to constrain the spatial distribution of the Lyα emission. As later shown

in Figure 1, Lyα emission for most of our sources is diffuse and extended. Although the Lyα flux measurements for our sources already exist in the literature (Richard et al. 2021), the values reported are severely underestimated (33-50%). Hence, to include most of the Lyα emission, including the diffuse low-surface brightness signal at the outskirts, we re-measured the fluxes and EWs. Details are described in the section below. We use rest-frame optical emission lines ([OIII]λ 5007, Hα, [O II], Hβ) from JWST/NIRSpec spectra to measure systemic redshifts and also line ratios to derive ionization, metallicity, and dust properties. The measured Hα and Hβ ratios enabled dust correction of the observed line fluxes to correctly estimate the Lyα $f_{esc}^{Ly\alpha}$ (see Table. 1). We start by describing the NIRSpec-derived quantities first.

3.1. *Rest-optical line measurements*

Rest frame optical emission lines of our LAE sample are obtained with the JWST NIRSpec spectroscopy. Data reduction pipeline steps, outlined in §2.2, produce wavelength & flux-calibrated, combined, rectified two-dimensional spectra for each slitlet. 1D spectrum and its associated error spectrum are extracted from the 2D spectrum using an optimal extraction algorithm (Horne 1986). Fig. 2 shows the Hα, [OIII], and [OII] lines for three example sources. We derive the systemic redshift from the [OIII] λ 5007Å emission line center and constrain all the other lines to have the same redshift in the given source. The fluxes and their uncertainties were derived for each emission line by fitting a Gaussian model, then dust corrected following the prescription outlined in §3.2 to produce the final flux ratio estimates reported in Table. 1. For calculating the ratio of Lyα output to the rest frame optical line flux, the optical fluxes need to be corrected by an additional slitloss fraction to compensate for the portion of the emission missed by the coverage of the NIRSpec slitless. The slitloss fraction is calculated as the fraction of the UV continuum light from within the NIRSpec slitlet open shutter area to the total light from the host galaxy boundary defined by the HST segmentation map. The slitloss fraction for our sources is not large and ranges between 0.55-0.78, which is encouraging, and dictates that our line ratios are representative of most of the gas in the galaxy.

3.2. *Dust correction*

We corrected the rest optical emission line fluxes for dust extinction using the Balmer decrement measurements. Assuming hydrogen lines emit from an optically thick HII region obeying Case B recombination, we considered the intrinsic Hα/Hβ ratio = 2.86. We adopted a Calzetti et al. (2000) extinction curve to compute the nebular color excess E(B-V). We took $k_{H\alpha}$ = 3.33 and $k_{H\beta}$ = 4.6. The corrected emission line fluxes are Line$_{corrected}$ = Line$_{obs}$ × $10^{0.4.E(B-V).k_\lambda}$ where k_λ is derived from the Calzetti et al.

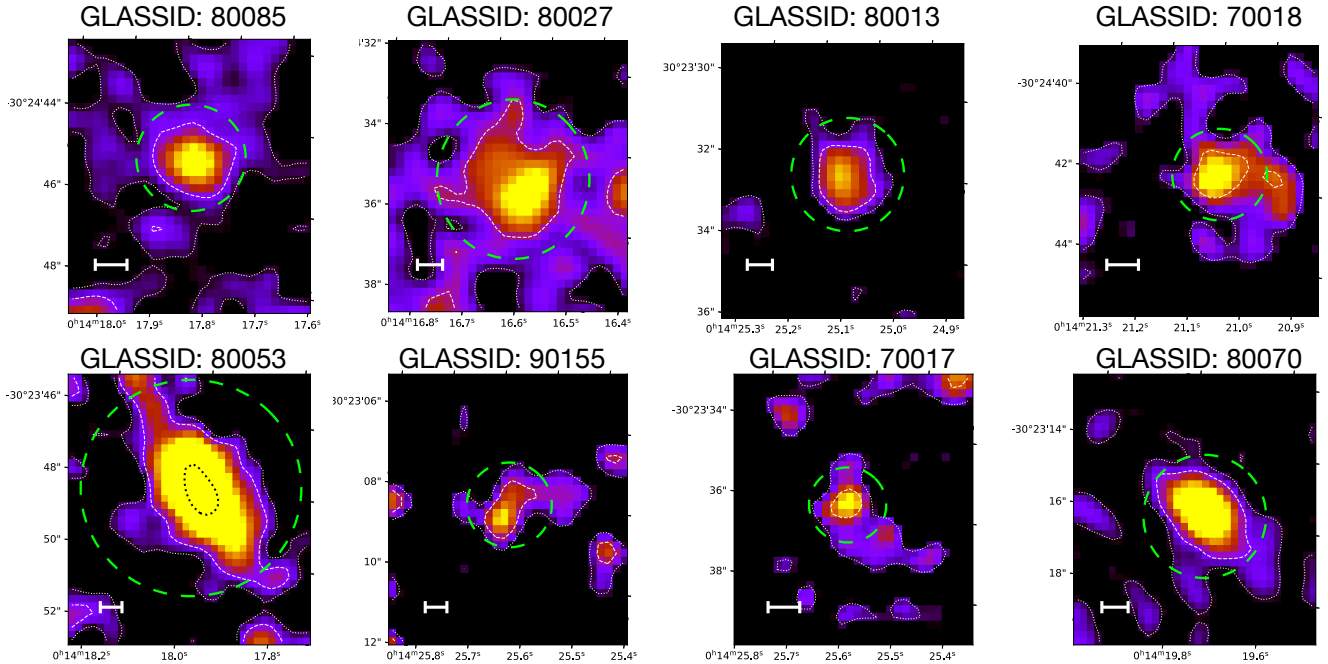**Figure 1.** 8 Lyα emitters out of the 11 objects we use for this study. Each panel shows a different object. The panels show Lyα narrowband image, constructed using the method described in §3.3. Overplotted on top are the surface brightness contours at 10^{-16} erg cm^{-2} s^{-1} arcsec^{-2} (black dotted line), 10^{-17} erg cm^{-2} s^{-1} arcsec^{-2} (white dashed line), and 10^{-18} erg cm^{-2} s^{-1} arcsec^{-2} (white dotted line). The radius of the green dashed circle corresponds to the CoG radius (see §3.4), which we used to obtain the total Lyα flux. The solid white line indicates 5 Kpc.

(2000) extinction curve at the wavelength of the specified line.

3.3. *Lyα narrow-band image construction*

We constructed pseudo-narrowband Lyα images using the MUSE datacube, each centered on the position and wavelength of the corresponding Lyα line. We closely followed the method designed by Leclercq et al. (2017). We used a wide spatial aperture to include all the detectable Lyα emissions above the noise level. The spectral bandwidths for constructing the Lyα NB image were chosen to include more than 95% of the total integrated Lyα line flux and to maximize the signal-to-noise within the $5'' \times 5''$ aperture of the said object. The chosen spectral bandwidths range between ~ 10 to 30 Å for our sources.

In this study, source crowding is a serious issue for many objects since almost all objects have projected close neighbors within a few arcseconds. However, these neighbors are typically at other redshifts than our chosen Lyα emitters, so they contaminate the NB signal only with continuum emission. To properly remove the continuum, we performed median filtering in the spectral direction in a wide window of 100 spectral pixels to ignore any emission lines in the MUSE data cube (similar to Herenz & Wisotzki 2017; Wisotzki et al. 2016; Leclercq et al. 2017). This produced a continuum-only data cube with all emission lines removed. A continuum-free data cube was then computed by subtracting this filtered data

cube from the original. The resulting Lyα images for 8 of our objects with SB contours at 10^{-16} (inner dotted white), 10^{-17} (dashed white), and 10^{-18} erg s^{-1} cm^{-2} arcsec^{-2} (outer dotted white) are shown in Fig. 1.

3.4. *Integrated Lyman-alpha flux and EW*

The Lyα flux was computed by integrating the datacubes inside the circular aperture corresponding to a radius known as the Curve of Growth radius or "CoG radius" (rCoG), similar to Leclercq et al. (2017). We averaged the flux in successive annuli of 1-pixel thickness around the emission center. The COG radius was determined by the annular radius for which the averaged flux reaches the noise value and the cumulative flux distribution flattens. The center of this last annulus corresponds to rCoG. From this aperture, we extracted a spectrum and integrated the flux corresponding to the Lyα line width; the borders of the line are set when the flux goes under zero. This method is more robust than using a single, fixed spatial aperture for all objects. This also ensured that most of the Lyα flux was included for each object. Note, due to this technique, our flux values are higher by a factor of $\sim$1.5-3 from the reported values in the public catalog of Richard et al. (2021). The extracted integrated spectrum for three example objects is shown in Fig. 2.

To calculate the EW, we needed to estimate the UV continuum at the wavelength of the Lyα line $f_{\mathrm{ly}\alpha}^{\mathrm{cont}}$. However, we do not detect any continuum from the MUSE spectra. Hence,

we utilize HST images mentioned in §2.4 to estimate the UV continuum slope and derive the continuum flux at 1216Å. These values are reported in Richard et al. (2021). The observed frame EW measurement (EW_z) is obtained by dividing the integrated line flux by the continuum flux. The rest frame EW is then given as EW = EW_z / (1+ z), where z is the redshift for the source.

3.5. *Lyα escape fraction*

To calculate the escape fraction, we implement a prescription similar to Hayes et al. (2005), which is = $L_{obs}^{Lyα}$/(8.7 × $L_{int}^{Hα}$). The case-B Lyα/Hα ratio is between 8.1 and 9.0. For consistency with previous studies, we use 8.7. Here, $L_{obs}^{Lyα}$ is the observed Lyα luminosity and $L_{int}^{Hα}$ is the intrinsic dust-corrected Hα luminosity. Corrected intrinsic Hα luminosity is given by: $L_{int}^{Hα} = L_{obs}^{Hα} × 10.\exp(0.4.E(B−V)$ (see §3.2 for details).

3.6. *Lyα FWHM and red peak velocity*

We non-parametrically characterize the full-width half maxima (FWHM) of the *red component of the Lyα emission* using the `specutils` package of python. We corrected the FWHM of the Lyα line for the spectral line spread function (LSF) of MUSE approximating the later as a Gaussian. The FWHM of the LSF is wavelength dependent, and we used the value for the MUSE-Deep Mosaic fields (with ten hours of exposure time) given by Bacon et al. (2017), which follows:

$$F_{mosaic} = 5.835 × 10^{-8}λ^{-2} − 9.080 × 10^{-4}λ + 5.983. \quad (1)$$

It should be kept in mind that the FWHM measurement becomes unreliable for narrow lines, which are dominated by the LSF (Verhamme et al. 2015, 2017). The red peak velocity of the Lyα profile is determined by measuring the velocity offset of the red component of the Lyα line relative to the systemic redshift of the sources. The systemic redshifts are determined from the brightest rest optical emission line ([OIII]λ5007Å) from the JWST NIRSpec spectra.

4. Lyα EMISSION IN Z > 3 MUSE LAE POPULATION

It is now well established that there is extended Lyα emission (or "halos") around individual LAEs (Wisotzki et al. 2016; Leclercq et al. 2017). Studies have found that the Lyα halo fraction goes up to 80-90% for UV-selected star-forming galaxies at high redshifts (2<z<5). Our sample is also no exception. Fig. 1 shows a representative sample of eight out of eleven galaxies in our sample. The white horizontal bar in each panel shows the physical length scale of 5 kpc. The spatial extent of the Lyα emission spans a large range, from 10 - 50 kpc. To quantify the extent of the diffuse emission, we plot the Lyα luminosity as a function of a distance ratio in Fig. 3 (upper left panel). The latter is defined as the ratio

of the COG radius indicating the spatial boundary of the Lyα emission (green dashed circles in Fig. 1) and the Petrosian radius of the galaxy containing 90% of the UV continuum flux (R_{90}). The ratio of these two measured quantities is always > 1 and varies from 1.5 - 9. This indicates that the Lyα emission of the galaxy is more extended spatially than the host galaxy's stellar light by several factors. The positive trend with the Lyα luminosity states that galaxies with more extended Lyα emission have a higher COG radius and produce a higher integrated Lyα output. The solid black line overlaid on top shows the best-fit relation with $1σ$ uncertainties indicated by the dashed blue lines. The extended Lyα emission implies that our sources have a significant amount of cool/warm gas in the CGM.

4.1. *Lyα spectral shape*

The Lyα profiles of three example galaxies out of the total 11 targets in our sample are shown in Fig. 2. We see a variety of spectral morphologies in the Lyα line. Most are very strong and relatively asymmetric, with more than one component. This diversity is consistent with previous observations of galaxies with strong Lyα emission (Kulas et al. 2012; Erb et al. 2014, 2016; Henry et al. 2015). At a spectral resolution of R ∼ 3000, we see double-peaked Lyα profiles in three out of 11 galaxies (i.e., 27%). Although a double-peaked profile is not ubiquitous in typical star-forming galaxies with Lyα observations (Östlin et al. 2014), they were found in 90% of the nearby (z<0.3) green pea population in Henry et al. (2015); Yang et al. (2017b). On the other hand, at higher redshift, Kerutt et al. (2022) found that 33% of objects below redshift 4 have a blue peak in Lyα emission, but that fraction drops to 16% for 4 < z < 5. The significant drop in the blue peak fraction at higher redshift is due to the rising neutral gas fraction in the intervening IGM, eating away the blue component and leaving only the red peak behind in the observed spectra. These are consistent with our high redshift sample at z = 3-6.

4.2. *Is our sample representative of the larger 3< z < 6 MUSE LAE population?*

Our primary goal in this study is to measure any correlation between $f_{esc}^{Lyα}$ and other physical properties facilitating $f_{esc}^{Lyα}$ for our z=3-6 LAE sample and to determine their similarity with the low redshift analog galaxies. First, we test whether our sample is representative of the larger population of high redshift LAEs in terms of Lyα output and host galaxy properties. We compare the Lyα EW vs. stellar mass of our sample (colored circles; each color indicating a source in Table. 1) to the MUSE z∼ 3- 6 LAEs (blue circles) drawn from the MUSE HUDF dataset (Bacon et al. 2023), mentioned in §2.5. As shown in Fig. 3 (middle panel), galaxies in our sample show the stellar mass and Lyα EW distribution to be extremely consistent with the HUDF sample while
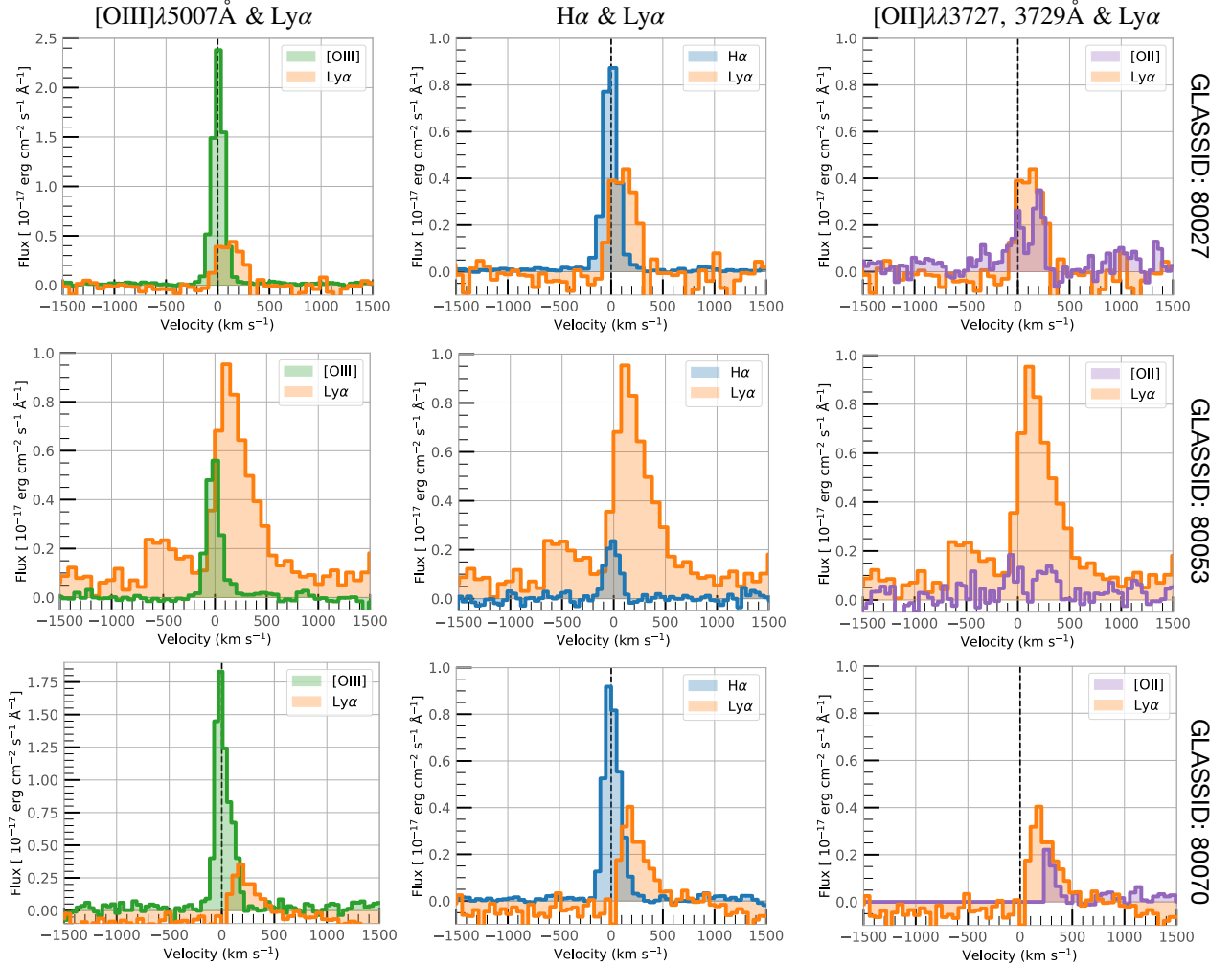
Figure 2. The Lyα line profiles extracted from the CoG radius from Fig. 1 are shown in orange with rest-frame optical emission lines overplotted for three example LAEs in our sample. The different rows indicate different galaxies. The emission lines shown are [OIII]λ 5007 in the first column (green), Hα in the second column (blue), and [OII]λλ3726, 3729 in the third column (purple).

covering a large range in stellar mass. There is also a clear negative correlation between the two quantities. Indeed, most observational studies of the stellar populations of Lyα galaxies suggest that the LAEs favor relatively young and low-mass systems (Ono et al. 2010; Hayes et al. 2023), although see Finkelstein et al. (2009) for counterexamples. This phenomenon occurs due to the increased gas and dust content of more massive galaxies, which makes Lyα escape difficult, thereby decreasing the measured Lyα EW. 9 out of 11 galaxies in our sample have stellar masses below $10^{9.5}$ $M_\odot$. Note that two galaxies in our sample have extremely low values of stellar mass with $M_\star < 10^{7.3}$ $M_\odot$. These two galaxies fall outside the range of the MUSE HUDF LAEs with well-constrained masses but may be consistent with the population of HUDF Lyα sources with little to no detected continuum in the HST imaging (Maseda et al. 2017).

In Fig. 3 (right panel), we show the star formation rate vs. the UV continuum luminosity measured at 1500Å. Our

sources occupy a similar region in the parameter space as the MUSE sample. Three sources show SFR > 2 $M_\odot$/yr, slightly higher than the typical values in the HUDF sample. This possibly arises from the different star formation rate estimators used in different catalog measurements. The positive correlation, seen in the figure, is expected since the SFR is derived from the UV luminosity estimates. The star formation rates of our sample vary between $\sim 0.1-10$ $M_\odot$/yr, which indicates a diverse population but representative of high z LAEs previously reported in the literature.

5. HOW DO THE LOW REDSHIFT ANALOG GALAXIES COMPARE WITH GALAXIES AT REDSHIFT > 3?

With the measurements of Lyα emission properties and the rest optical emission line ratios, we are ready to investigate how our high z LAE sample compares with the low
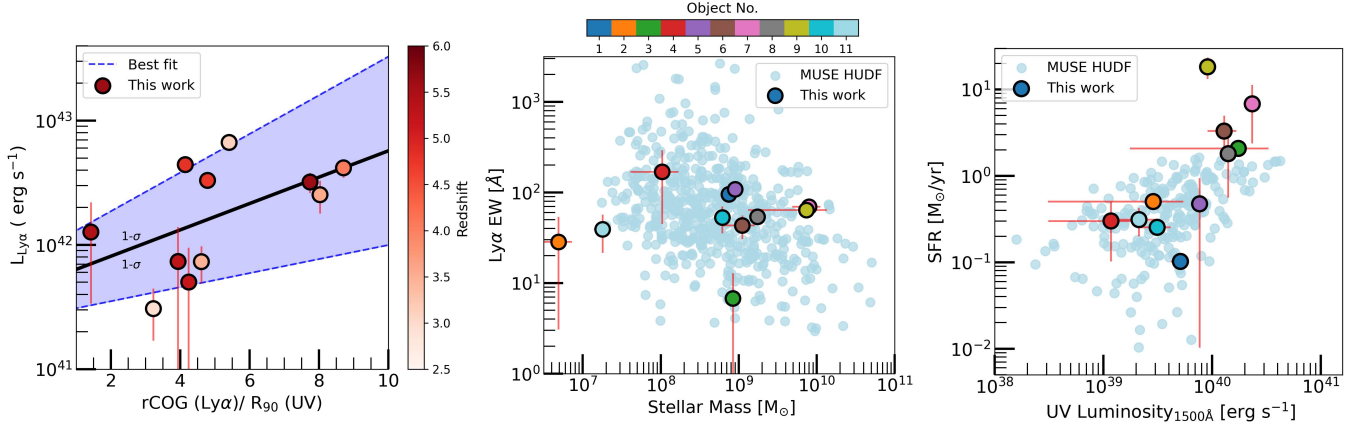
Figure 3. *Left:* The total Lyα luminosity measured from the Lyα NB images (Fig. 1) as a function of the ratio of COG radius (green circles in Fig. 1) and Petrosian radius at 90% stellar light. The black dashed line shows the best-fit relation, with 1σ uncertainty in purple. The sources are color-coded by redshift. *Middle:* Lyα EW vs.stellar mass for our sample of 11 LAEs (colored circles) compared against the z∼ 3-6 LAEs from the MUSE Hubble Ultra Deep Field (HUDF) survey in blue (Bacon et al. 2023). Each of our sources is assigned a specific color (see Table. 1). *Right:* SFR vs. UV luminosity measured at rest frame 1500Å wavelength for our sources (colored circles) and the MUSE HUDF sources (blue circles). Our chosen sample is largely consistent with the larger population of z>3 MUSE HUDF sample in terms of stellar mass, SFR, UV luminosity, and Lyα EW. Our small number of galaxies is thus representative of z∼ 3 LAEs.

redshift analogs and LyC emitters (Hayes et al. 2023; Flury et al. 2022).

5.1. *Lyα FWHM vs. red peak velocity*

With the availability of the JWST NIRspec spectra, we can measure the systemic redshift of our z> 3 sources based on the brightest rest optical emission lines. This enables us to determine the Lyα red peak velocity offset with confidence. In Fig. 4 in the top left panel, we show the FWHM of the Lyα profiles as a function of the velocity offset for our targets. Our 3< z < 6 LAE sources are shown in circles, with each color indicating a different source, as listed in Table. 1. The blue squares indicate the z<0.5 galaxies, which are analogs to the high z LAEs (sample from Hayes et al. 2023). We find a strong positive correlation between the velocity and FWHM in our sample, echoing the trend observed with the low redshift analog galaxies. This is also in strong agreement with the prediction from the radiative transfer (RT) theory, which states that low, neutral hydrogen column density causes Lyα photons to scatter less and thus helps them to escape more easily. This shapes the Lyα line to be narrower (low FWHM), brighter (enhanced flux), and less redshifted (low-velocity offset) compared to the systemic velocity.

This similarity between the low z and high z samples and their agreement with the RT models suggests that the mechanisms regulating the output of Lyα may not vary with redshift. The mean red peak velocity for our sample is 207 ± 53 km s^{-1}. This is consistent with the measurements from the low-z analogs, with a mean velocity = 241 km s^{-1}. This strong positive correlation for z> 3 galaxies indicates that these properties may be related intrinsically in $z > 6$ galaxies as well, although both are impacted by neutral IGM

gas at these redshifts. This empirical relation can be used to derive the systemic redshifts of even higher redshift galaxies from the measurement of the FWHM of the Lyα line alone.

5.2. *Lyα escape fraction*

We estimate the escape fraction of Lyα photons reaching the detector from the Lyα/Hα flux ratio, as described in §3.5. We find that the escape fraction varies between 0.02 - 0.26, with a mean $f_{esc}^{Ly\alpha} = 0.10 \pm 0.03$, which is slightly lower than the low redshift population (mean $f_{esc}^{Ly\alpha} = 0.23$). High redshift LAEs from existing studies find a large range of escape fraction: Hayes et al. (2010) find $f_{esc}^{Ly\alpha} \sim 0.05$ while Steidel et al. (2011) reports $f_{esc}^{Ly\alpha} \sim 0.3$ for z∼ 2 LAEs. Trainor et al. (2015) also estimate an escape fraction of ∼ 30% for a sample of faint LAEs at z ∼ 2.7. However, we should note that many of these previously existing studies of z> 2 LAEs lacked rest-optical spectra with sufficient sensitivity to measure Hα flux and correctly perform dust correction. The $f_{esc}^{Ly\alpha}$ values for our sample are listed in Table. 1 and are plotted against Lyα EW in the upper middle panel of Fig. 4 (circles). The low redshift analogs and the LzLCs samples are also shown using squares and triangles, respectively. The two quantities show a positive correlation for our sources and are consistent with the values seen in the low redshift LAEs. Five of our galaxies show a Lyα escape fraction >10%. Interestingly, the low-redshift samples show some spread in Lyα EW for a given $f_{esc}^{Ly\alpha}$, which could be related to the stellar population properties. Multiple factors like initial mass function, metallicity, or the presence of binaries can make the ionizing spectrum to be harder, which can produce more ionizing photons, and therefore Lyα photons, for a given non-ionizing UV luminosity (Malhotra & Rhoads 2002). Compared to the

low-z analogs, our sample falls more towards the higher EWs for a given $f_{esc}^{Ly\alpha}$, which could indicate more extreme stellar populations in the $z > 3$ galaxies.

In general, when the column density of the gas is low, Lyα photons scatter much less - resulting in smaller velocity offsets and greater Lyα escape. A similar relationship is also seen in the Lyman continuum leakers. Lower velocity offsets exhibit broader lines, a greater Lyman continuum escape, and a greater Lyα escape fraction (Izotov et al. 2018). Thus, we expect a negative trend between the velocity offset and the Lyα escape fraction. We show the relation between these two quantities for our objects (circles) in the upper right panel in Fig. 4, compared with the low redshift analog galaxies (squares). Taken alone, our sample does not show any trend, and there is a considerable scatter in our high z sources. A larger sample can provide better inference on the validity of this relation for high redshift galaxies.

5.3. *Galaxy morphology*

The concentrated star formation and high SFR surface densities are necessary for producing an ample amount of ionizing radiation, thus, creating excess Lyα photons. Hence, compact, highly star-forming galaxies host strong Lyα emissions. Indeed, our sample of z>3 LAEs is sufficiently compact in UV continuum size, as observed from the HST/ACS images. Our sample's mean effective radius (R_e) is ~ 1.1 kpc, with some galaxies exhibiting R_e as low as 0.1 kpc. This is expected since galaxies with strong Lyα emission likely represent galaxies in earlier stages of evolution with younger ages and smaller sizes. The effective sizes of our sources are given in Table, 1. This finding is also qualitatively consistent with that of Malhotra et al. (2012), and Hayes et al. (2023). They found that LAEs, in general, are drawn from the more compact end of the size distribution of normal star-forming galaxies. Quantitatively, Malhotra et al. (2012) find LAEs to have half-light radii close to 1.0 kpc at redshifts 2–6, which is in remarkable agreement with our measurement of the effective radius.

5.4. *Variation of [OIII]/[OII] ratio with Lyα escape fraction*

The [OIII]λ5007Å/[OII]λ3727,29 Å ratio (or O_{32}, in short) measures the ionization state of the gas in a galaxy. A classical HII region model uses two zones. If the neutral gas gets sufficiently depleted due to the ionizing photons from young stars, the outer edge of the HII regions gets truncated. This reduces the [OII] emission, resulting in a high O_{32} ratio. This scenario indicates low, neutral gas column density channels that allow Lyα and Lyman continuum photons to escape more easily. Thus a high O_{32} ratio has been proposed to trace "density-bounded" neutral gas regions in Lyα emitting galaxies, which can generate a lot of ionizing radiation, and thus a lot of Lyα photons (Jaskot & Oey 2013; Nakajima & Ouchi 2014).

Izotov et al. (2016) found observational evidence for the first time that high O_{32} ratios are a potential signature of Lyman continuum leakage and can trace a low-density path through the interstellar medium of galaxies along the line of sight. Similarly, Nakajima et al. (2013); Nakajima & Ouchi (2014) found that galaxies with a high O_{32} ratio in low redshift analog populations like the green peas, Lyman break analogs, and in high redshift z = 2–3 galaxies have a high Lyα escape fraction. Figure. 4 lower left panel shows the O_{32} ratio as a function of the Lyα escape fraction for our sample (circles). We show the Low redshift Lyman continuum survey (LzLCS) galaxies from Flury et al. (2022) (green triangles), and low redshift analog galaxies from Hayes et al. (2023) (blue squares) for comparison. The LzLCs sample and the low z analog galaxies show a positive trend between the two quantities. In our sample, only 6 out of 11 galaxies have simultaneous detection of both [OIII] and [OII] emission lines to derive the O_{32} ratio. Our sources have O_{32} ratio between 2.5-14.1 and are overall consistent with the positive correlation between [OIII]/[OII] and $f_{esc}^{Ly\alpha}$ seen in the low redshift analog galaxies. Establishing this correlation at high redshift is crucial since O_{32} is one of the key diagnostics available to JWST at $z > 7$.

5.5. *Ionization and metallicity*

Gas-phase metallicity is a key property of the host galaxy ISM since it is a record of a galaxy's star formation history and gas infall/outflow. Metallicity estimates can be made with metal lines divided by hydrogen recombination lines, such as ([O III] $\lambda\lambda$ 5007, 4959 + [O II] $\lambda3727$)/Hβ (R_{23} index; Pagel et al. 1979; Kewley & Dopita 2002). Cowie et al. (2011) found that low redshift LAEs exhibit lower metallicities, compact sizes, and younger ages compared to a UV-continuum-selected sample of star-forming galaxies at similar stellar mass and redshift. These findings are consistent with the idea that LAEs are galaxies in the early stages of evolution. On the other hand, the ionization state, traced by O_{32}, is sensitive to the degree of excitation and the optical depth of the HII region in a galaxy (e.g., Brinchmann et al. 2008); a large O_{32} may be due to a low optical depth and a high escape fraction of ionizing photons, as discussed in the previous section. Nakajima et al. (2013); Nakajima & Ouchi (2014), for the first time, presented the ionization and metal properties for a very small sample of z∼ 2 LAEs based on multiple nebular emission lines. They found that the high z LAEs have a higher typical ionization parameter and lower metallicity in contrast with other high z galaxies.

We show the relationship between the O_{32} and the R_{23} index (Fig. 4 lower middle panel) for our sources in circles, compared with the low redshift analog population: Hayes et al. (2023) (blue squares) and low redshift Lyman Continuum emitters Flury et al. (2022) (green triangles). Our
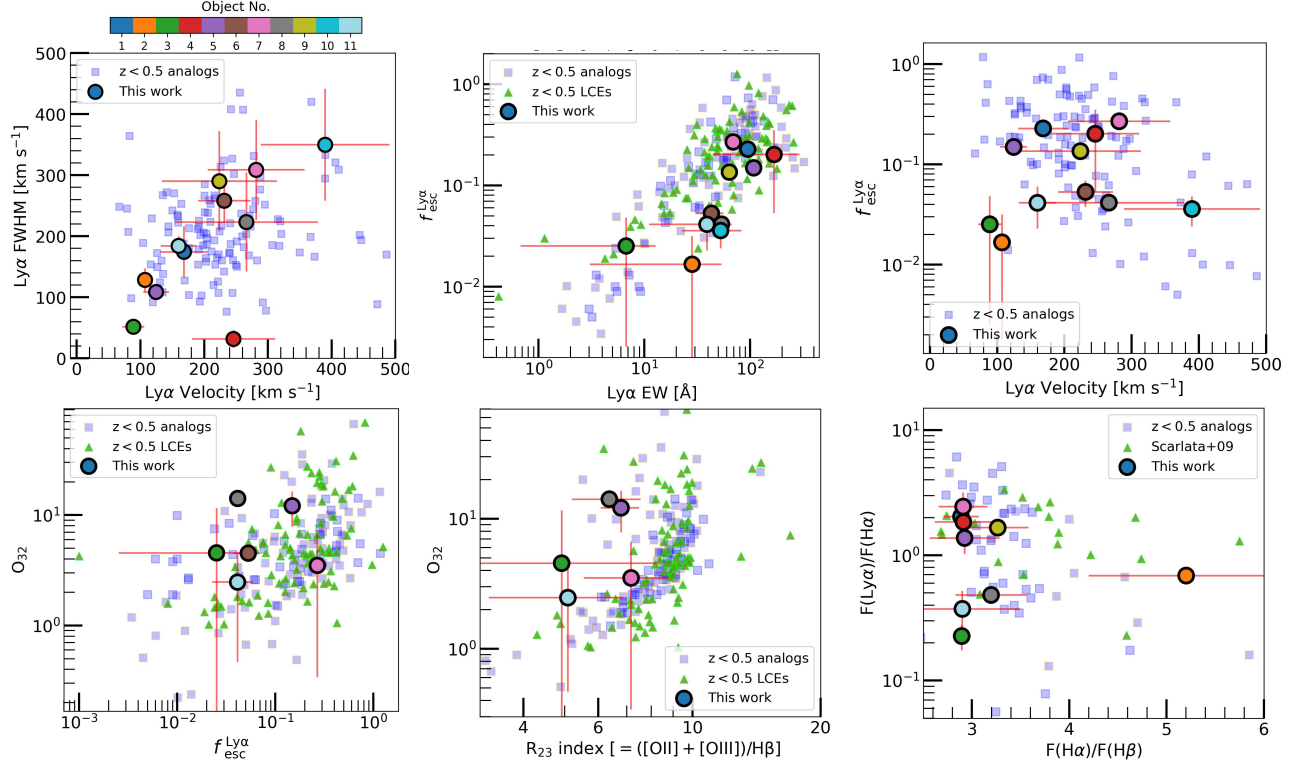
Figure 4. *Upper left:* FWHM of the red peak of Lyα vs. red peak velocity offset for all 11 sources in our study (colored circles) compared to the low-z analog sample from Hayes et al. (2023) (blue squares). The velocity offsets are calculated with respect to the systemic velocity measured from the JWST/NIRSpec spectra. Each of our objects is assigned a specific color, as indicated in the color scale. The object identifier numbers correspond to the numbers quoted in the first column of Table. 1. *Upper middle:* Lyα escape fraction vs. Lyα EW for our sources (circles) compared with the low z analog galaxies (Hayes et al. 2023) (blue squares) and low redshift Lyman continuum emitters from the LzLCs survey (Flury et al. 2022) (green triangles). *Upper right:* Lyα escape fraction vs. velocity offset. Symbols and colors are the same as in the previous panel. *Lower left:* O_{32} ratio vs. Lyα escape fraction for our sources with detected [OIII] *and* [OII] emission lines (circle). Low z analog galaxies (Hayes et al. 2023) and low z Lyman continuum emitters (Flury et al. 2022) are shown in blue squares and green triangles, respectively. *Lower middle:* O_{32} ratio vs. R_{23} index, which is defined as ([OII] + [OIII])/Hβ. R_{23} is a metallicity indicator. Symbols and comparison samples are the same as in the middle panel. *Lower right:* Lyα/Hα vs. Hα/Hβ ratio for our sample (red circles) compared with low z analogs (Hayes et al. 2023, blue squares;) and GALEX grism selected dusty LAEs (green triangles; Scarlata et al. 2009). See text for details.

sources occupy a broad region in the O_{32} vs. R_{23} parameter space, although the uncertainty of the measurements is also considerably high. This large scatter in the O_{32} vs. R_{23} diagram has also been seen with other Lyα emitters at z > 4 using JWST measurements (Mascia et al. 2023). This could imply that high redshift LAEs exhibit a vast range of metallicity and ionization states of the gas, or it could simply be an effect of large uncertainties in the measurements.

5.6. *Dust extinction and reddening*

The effect of dust content on Lyα emission has been studied extensively (Scarlata et al. 2009; Finkelstein et al. 2011; Hayes et al. 2010; Cowie et al. 2011; Nakajima et al. 2012; Henry et al. 2015). Lyα photons produced from the star-forming regions can undergo multiple scattering from the HI gas in the ISM and CGM of galaxies. With the increase in the number of scattering, the probability of the Lyα photons to be absorbed by dust grains also increases. Thus, the observed line intensities depend on the number of ionizing photons and

the attenuation produced by dust along the line of sight. High dust content indicates low Lyα output.

In Fig. 4 lower right panel, we show the Lyα/Hα flux ratio as a function of the observed Hα/Hβ ratio for our objects. Comparing our sample with other Lyα emitting galaxies with published Lyα and optical line ratio measurements is crucial. We separate the low z analog sample into two groups – galaxies identified as "dusty" LAEs from GALEX grism surveys (Scarlata et al. 2009) shown in green triangles, and the rest of the low redshift analog galaxies from Hayes et al. (2023), shown in blue, that include galaxies from the Lyα reference survey (Hayes et al. 2013, 2014), green pea population (Yang et al. 2017b), blueberries (Yang et al. 2017a) and Lyman Break Analogs (Heckman et al. 2015). In the absence of dust, for case B recombination at $T_e \sim 10^4$ K and $n_e = 10^2$ cm^{-3}, the expected line ratios are 2.86 and 8.7 for Hα/Hβ and Lyα/Hβ ratios respectively (Pengelly 1964). Galaxies in our sample show a large range in Lyα/Hα, but a comparatively small range in Hα/Hβ. The mean Hα/Hβ

ratio is 3.2±1.3, indicating low dust content. This is similar to the low z analog galaxies, where 90% of the population has Hα/Hβ < 4. 9 out of 11 sources have simultaneous detection of both Hα and Hβ, while the other two sources miss Hβ line due to detector gaps. 8 out of those 9 galaxies have Hα/Hβ <3.3 and are greatly consistent with the low redshift analogs, particularly the Green pea population (Henry et al. 2015; Yang et al. 2017b). One galaxy shows a very high dust content with a value of 5.2, which is more consistent with the local dusty LAEs of Scarlata et al. (2009), shown in Figure. The low dust content for the LAEs is consistent with the prediction that a higher amount of dust content scatter and absorbs the Lyα photons more, making their escape difficult. The Lyα/Hα ratio for all our sources is smaller than the value of 8 - 9 predicted from case B. They vary by almost an order of magnitude. 7 of our high z LAE sources show Lyα/Hα overall consistent with the low redshift population. The remaining two sources have considerably low Lyα output.

6. DISCUSSION

6.1. *Comparison with low z analogs and LyC leakers*

Lyα is possibly the best indirect diagnostic of LyC escape since the conditions that favor the escape of Lyα photons are often the same that allow for the escape of LyC photons. In this work, we concentrate on studying Lyα emission for galaxies with z < 6, thus avoiding the significant IGM attenuation but being close enough in redshift to the EoR. We study the correlations between $f_{esc}^{Ly\alpha}$ with another indirect but promising diagnostic tested at low redshift by (Flury et al. 2022): O_{32}. One of our primary goals is to determine whether the correlations observed in the low-z population prevail in the z = 3 - 6 regime as well. We compare our sample with two main low z samples – 1) low z "analogs" from Hayes et al. (2023) - which include green peas, blueberries, Lyman break analogs, intense starbursts, and extreme emission line galaxies, and 2) low redshift Lyman continuum emitters from Flury et al. (2022), which are candidates for LyC leakers.

In Fig. 4, we plot the relation between $f_{esc}^{Ly\alpha}$ with Lyα EW, velocity offset, and O_{32} for our JWST high redshift sample and compare them with the local population (Hayes et al. 2023; Flury et al. 2022). A huge caveat for our study is the small size of our sample. The objects in our sample do not show any strong correlations by themselves. Here we discuss if they are generally consistent with the correlation parameter space occupied by the low redshift galaxies.

We find that the $f_{esc}^{Ly\alpha}$ vs. Lyα EW generally shows a positive trend, as expected. However, two sources (Object 8, 10) show lower $f_{esc}^{Ly\alpha}$ than expected for the given Lyα output. One of them (Object 8) shows a higher dust content which might contribute to the lower $f_{esc}^{Ly\alpha}$. We next analyze the $f_{esc}^{Ly\alpha}$ vs velocity offset. Our sources are consistent with the Hayes et al. (2023) low-redshift analogs, although there is a significant

scatter. Our systemic redshift measurements are determined from the brightest rest optical lines (Hα and [OIII]5007Å) measured from the NIRSpec spectra. Uncertainties in wavelength calibration in JWST/NIRSpec and MUSE spectra can contribute to this scatter. However, two sources (Object 2 and 3) have the lowest $f_{esc}^{Ly\alpha}$ and Lyα velocity and hence lie completely offset from the low z analogs. These are also two of our sample's highest redshift galaxies (z = 5.186 and 5.282). We hypothesize that this could be caused by IGM attenuation.

We now focus on O_{32}. High O_{32} has been proposed as an indicator of higher f_{esc} (e.g., Nakajima & Ouchi 2014). The reasoning is that the high O_{32} ratio selects highly ionized systems, which are more likely to have density-bounded channels through which ionizing photons can escape. We do not have a direct estimate of LyC f_{esc}, so we plot O_{32} vs. $f_{esc}^{Ly\alpha}$. We find that all 6 sources of our sample with measured O_{32} indeed mostly lies in the region of the plot populated by low-redshift LyC leakers (Flury et al. 2022) and analogs sample (Hayes et al. 2023). The median O_{32} is 4.5 ± 1.2. We see that the majority of our sources (4 out of 6 galaxies) show $O_{32} < 5$, which has been indicated as a lower threshold for LyC leakers with an $f_{esc} > 0.05$ (Flury et al. 2022). Thus our objects are predicted to have $f_{esc} < 0.05$. Although, some studies have shown that O_{32} does not necessarily correlate well. with f_{esc} (Naidu et al. 2018; Katz et al. 2020), and thus are not expected to correlate with $f_{esc}^{Ly\alpha}$ as well; nonetheless, samples of LyC leaking galaxies at low-redshift generally show that the fraction of galaxies with high f_{esc} increase toward higher O32, even if the correlation is not tight (e.g., Izotov et al. 2016; Flury et al. 2022). This is precisely what we find in our sample with $f_{esc}^{Ly\alpha}$ as well.

Finally, the O_{32} vs R_{23} index diagram is widely used to examine the gas-phase metallicity and ionization state both in the local universe (e.g., Izotov et al. 2016, 2018) and at high redshift (Flury et al. 2022; Nakajima et al. 2020; Reddy et al. 2022; Vanzella et al. 2019). Recent studies by Nakajima et al. (2020) showed that z ∼ 3 LyC leakers tend to populate the upper right part of this diagram, i.e., they have high O_{32} and high R_{23}. This result is also seen in high-resolution cosmological radiation hydrodynamics simulations (Katz et al. 2020). However, both these studies conclude that the O_{32} vs R_{23} plane is not the most useful to differentiate between leakers and non-leakers. Our sample occupies a broad region in the parameter space, which could reflect either a wider range of metallicity and ionization states or the fact that we have a large measurement uncertainty, very similar to 4.5 < z < 8 Lyα emitting galaxies studied by (Mascia et al. 2023).

6.2. *Prediction of LyC escape fractions*

We try to indirectly estimate f_{esc} from our measured properties. Previous studies have attempted to estimate f_{esc} based

Table 1. Lyα and rest-optical properties of $z \sim 3 - 6$ galaxies in the GLASS-JWST program used in this work.

No.	ID	R_e (kpc)	z_{sys}	$V_{Ly\alpha}$ (km/s)	$FWHM_{Ly\alpha}$ (km/s)	$F_{Ly\alpha}$ (10^{-20} erg cm^{-2} s^{-1})	Lyα EW (Å)	$f_{esc}^{Ly\alpha}$	O_{32}*	F(Lyα)/F(Hα)**	F(Hα)/F(Hβ)**	R_{23}*
1	70003	0.12	5.618	168 ± 37	174 ± 41	941.1 ± 173.7	95 ± 17	0.23 ± 0.04	–	2.0 ± 0.4	2.89 ± 0.18	–
2	70017	0.33	5.186	107 ± 5	128 ± 19	177.7 ± 158.5	28 ± 25	0.02 ± 0.01	–	0.7 ± 0.0	5.2 ± 1.18	–
3	70018	0.77	5.282	89 ± 17	51 ± 10	249.2 ± 224.1	6 ± 6	0.03 ± 0.02	4.5 ± 6.0	0.2 ± 0.1	2.89 ± 0.09	4.9 ± 3.3
4	70022	3.34	5.429	245 ± 65	31 ± 14	403.5 ± 296.7	168 ± 123	0.2 ± 0.15	–	1.8 ± 0.5	2.91 ± 0.29	–
5	80013	0.7	4.043	124 ± 20	108 ± 12	2653.7 ± 444.1	108 ± 18	0.15 ± 0.02	12.1 ± 4.3	1.4 ± 0.3	2.92 ± 0.36	6.8 ± 0.7
6	80027	0.92	3.58	231 ± 41	257 ± 36	2154.8 ± 632.4	43 ± 12	0.05 ± 0.02	4.5 ± 0.2	0.6 ± 0.1	–	–
7	80053	1.55	3.129	281 ± 76	308 ± 82	7829.7 ± 705.2	69 ± 6	0.27 ± 0.02	3.5 ± 3.2	2.4 ± 0.7	2.91 ± 0.25	7.2 ± 1.6
8	80070	0.9	4.797	266 ± 112	223 ± 80	1881.0 ± 236.8	54 ± 9	0.04 ± 0.01	14.1 ± 0.8	0.5 ± 0.1	3.2 ± 0.37	6.4 ± 1.1
9	80085	0.8	4.725	223 ± 90	289 ± 81	1454.9 ± 193.8	63 ± 8	0.14 ± 0.02	–	1.7 ± 0.2	3.26 ± 0.32	–
10	80113	0.95	3.472	389 ± 101	349 ± 91	669.6 ± 221.3	53 ± 17	0.04 ± 0.01	–	0.4 ± 0.1	–	–
11	90155	0.7	2.94	159 ± 28	184 ± 15	418.0 ± 187.1	39 ± 18	0.04 ± 0.02	2.5 ± 2.0	0.4 ± 0.1	2.9 ± 0.59	5.1 ± 1.8

NOTE— No. indicates Object Serial number matching the color scale in Fig. 3 & 4. * O_{32} and R_{23} denotes the dust corrected ratio of ([OIII]λ5007Å/[OII] λ3727, 29Å) and ([OIII]λ5007 + [OII]λ3727, 39) / Hβ respectively. For sources where Hβ falls in the detector gaps, we perform dust correction assuming a mean E(B-v) = 0.09. **Observed flux ratios.

on neutral gas properties and low ionization absrobtion lines. It is difficult to detect such lines and obtain neutral gas properties at higher redshifts. Hence, we adopt the fully-data driven regression analysis on observable galaxy properties, presented by Mascia et al. (2023), for a similar sample of z = 4-8 Lyα emitting galaxies in the GLASS dataset. Note that Mascia et al. (2023) used the low redshift Lyman continuum survey to derive this relation and then applied it to z = 4-8 LAEs. The best-fit relation they proposed is:

$$\log_{10}(f_{esc}) = A + B * \log_{10}(O_{32}) + C * r_e + D * \beta \quad (2)$$

Where A = -1.92, B = 0.48, C = -0.96, D = -0.41, r_e is the effective radius in kpc (Table. 1) and β is the mean UV slope = -2.3±0.4, calculated by Prieto-Lyon et al. 2023 (in prep). We find that the f_{esc} varies between 0.03 - 0.07 with a mean value = 0.04. This is consistent with what we previously hypothesized – the majority of our sources should have $f_{esc} < 0.05$ based on the O_{32} ratio alone. The main limitation of our study is the small sample size. Our results are mostly based on 6 sources with the detection of both [OIII] and [OII] lines. A larger and more evenly distributed sample would be required to draw any conclusion. Still, our f_{esc} is rather low, with the average value lower than the median $f_{esc} \sim 0.1$ predicted by Naidu et al. (2020) and Mascia et al. (2023) for galaxies with median z = 6.

7. SUMMARY

Thanks to the deep spectroscopic data obtained with MUSE and the outstanding JWST NIRSpec spectroscopy on selected targets in the field of the Abell 2744 cluster: we have been able to study the rest frame UV-optical spectral properties of 11 Lyα emitting galaxies with spectroscopic redshift in the range $3 < z < 6$. We aimed to answer how the Lyα emission and their correlations with the galaxy properties compare between our high redshift sample with the existing low redshift analog population. Using the combined analyses of JWST NIRSpec and MUSE spectra, we were able to measure accurate estimates of systemic redshifts, Lyα velocity offsets, $f_{esc}^{Ly\alpha}$, ionization states, metallicity indicators, and dust content. We report the measurements of the most prominent rest optical emission lines (Hα, [OIII], [OII], Hβ). Our main results are summarized as follows:

1. All 11 galaxies in our sample are detected to have diffuse extended Lyα emission. We find a large range of physical sizes of these extended Lyα emissions ranging from 10 - 50 kpc, often extending beyond the host galaxy's stellar component (similar to Leclercq et al. 2017; Hayes et al. 2013). Our Lyα spectral profiles show a diverse morphology, with 3/11 showing a double-peaked profile.

2. The full-width half maxima of the Lyα emission shows positive correlations with the Lyα red peak velocity offset. Thus, the low-z derived relation works well for z< 6 galaxies and can be used to estimate systemic redshifts based on measurements of Lyα FWHM alone, as previously proposed by Verhamme et al. (2017).

3. We compared our 11 galaxies to the low redshift LyC emitters from Flury et al. (2022) and low redshift analogs from Hayes et al. (2023). Although our galaxies do not show many strong correlations if taken alone, their properties are entirely consistent with the low redshift population in terms of Lyα EW, $f_{esc}^{Ly\alpha}$, O_{32}, Lyα/Hα and dust content.

4. Our high z LAE sample has low dust content (all except three have Hα/Hβ< 3), compact sizes (mean $R_e \sim 1$ kpc), low mass ($M_\star < 10^{10}$ $M_\odot$) and high SFR (SFR ~ 0.1 - 10 $M_\odot$/yr). These are consistent with the prediction from radiative transfer models and imply that Lyα emitting galaxies define the early stages of a galaxy's lifecycle. The low dust allows the Lyα photons to escape without being completely absorbed. The striking similarity of the Lyα/Hα ratio vs. Balmer decrement with the low redshift analog population is remarkably evident even for our small sample of sources.

5. We use the empirical relation between LyC escape fraction and the three galaxy parameters proposed by Mascia et al. (2023), to predict LyC f_{esc}. We find that our sources are not strong LyC leakers, with an average LyC escape fraction ~ 0.04.

In conclusion, our low mass high redshift galaxies have physical and spectroscopic properties to be broadly consistent with the low redshift population, which are rightly considered "analogs" of high redshift LAEs. This suggests that diagnostic relations for Lyα and LyC, derived using low-z analogs (Flury et al. 2022; Runnholm et al. 2020), may be applicable in early epochs. With the caveat of a small sample size, we found that the amount of escaping ionizing photons is not large in our galaxies ($f_{esc} \sim 0.03$ - 0.07). A larger sample covering a wider range in redshift, stellar mass, and SFR is needed to make a stronger statement about the nature of correlations seen in the high z

LAEs. Larger JWST samples taken, for example, from the JWST JADES GTO program, will be suitable for studying more high redshift LAEs and better calibrating the correlations we show here.

REFERENCES

Ahumada, R., Allende Prieto, C., Almeida, A., et al. 2020, ApJS, 249, 3, doi: 10.3847/1538-4365/ab929e

Bacon, R., Conseil, S., Mary, D., et al. 2017, A&A, 608, A1, doi: 10.1051/0004-6361/201730833

Bacon, R., Brinchmann, J., Conseil, S., et al. 2023, A&A, 670, A4, doi: 10.1051/0004-6361/202244187

Boyett, K., Trenti, M., Leethochawalit, N., et al. 2023, arXiv e-prints, arXiv:2303.00306, doi: 10.48550/arXiv.2303.00306

Brinchmann, J., Pettini, M., & Charlot, S. 2008, MNRAS, 385, 769, doi: 10.1111/j.1365-2966.2008.12914.x

Bunker, A. J., Saxena, A., Cameron, A. J., et al. 2023, arXiv e-prints, arXiv:2302.07256, doi: 10.48550/arXiv.2302.07256

Calzetti, D., Armus, L., Bohlin, R. C., et al. 2000, ApJ, 533, 682, doi: 10.1086/308692

Cameron, A. J., Saxena, A., Bunker, A. J., et al. 2023, arXiv e-prints, arXiv:2302.04298, doi: 10.48550/arXiv.2302.04298

Cardamone, C., Schawinski, K., Sarzi, M., et al. 2009, MNRAS, 399, 1191, doi: 10.1111/j.1365-2966.2009.15383.x

Castellano, M., Amorín, R., Merlin, E., et al. 2016, A&A, 590, A31, doi: 10.1051/0004-6361/201527514

Chisholm, J., Prochaska, J. X., Schaerer, D., Gazagnes, S., & Henry, A. 2020, MNRAS, 498, 2554, doi: 10.1093/mnras/staa2470

Cowie, L. L., Barger, A. J., & Hu, E. M. 2011, ApJ, 738, 136, doi: 10.1088/0004-637X/738/2/136

Curti, M., D'Eugenio, F., Carniani, S., et al. 2023, MNRAS, 518, 425, doi: 10.1093/mnras/stac2737

Curtis-Lake, E., Carniani, S., Cameron, A., et al. 2022, arXiv e-prints, arXiv:2212.04568, doi: 10.48550/arXiv.2212.04568

Erb, D. K., Pettini, M., Steidel, C. C., et al. 2016, ApJ, 830, 52, doi: 10.3847/0004-637X/830/1/52

Erb, D. K., Steidel, C. C., Trainor, R. F., et al. 2014, ApJ, 795, 33, doi: 10.1088/0004-637X/795/1/33

Finkelstein, K. D., Papovich, C., Finkelstein, S. L., et al. 2011, ApJ, 742, 108, doi: 10.1088/0004-637X/742/2/108

Finkelstein, S. L., Cohen, S. H., Malhotra, S., & Rhoads, J. E. 2009, ApJ, 700, 276, doi: 10.1088/0004-637X/700/1/276

Finkelstein, S. L., D'Aloisio, A., Paardekooper, J.-P., et al. 2019, ApJ, 879, 36, doi: 10.3847/1538-4357/ab1ea8

Flury, S. R., Jaskot, A. E., Ferguson, H. C., et al. 2022, ApJS, 260, 1, doi: 10.3847/1538-4365/ac5331

Fujimoto, S., Arrabal Haro, P., Dickinson, M., et al. 2023, arXiv e-prints, arXiv:2301.09482, doi: 10.48550/arXiv.2301.09482

Fuller, S., Lemaux, B. C., Bradač, M., et al. 2020, ApJ, 896, 156, doi: 10.3847/1538-4357/ab959f

Gazagnes, S., Chisholm, J., Schaerer, D., Verhamme, A., & Izotov, Y. 2020, A&A, 639, A85, doi: 10.1051/0004-6361/202038096

Hayes, M., Östlin, G., Mas-Hesse, J. M., et al. 2005, A&A, 438, 71, doi: 10.1051/0004-6361:20052702

Hayes, M., Östlin, G., Schaerer, D., et al. 2010, Nature, 464, 562, doi: 10.1038/nature08881

—. 2013, ApJL, 765, L27, doi: 10.1088/2041-8205/765/2/L27

Hayes, M., Östlin, G., Duval, F., et al. 2014, ApJ, 782, 6, doi: 10.1088/0004-637X/782/1/6

Hayes, M. J., Runnholm, A., Scarlata, C., Gronke, M., & Rivera-Thorsen, T. E. 2023, MNRAS, 520, 5903, doi: 10.1093/mnras/stad477

Heckman, T. M., Alexandroff, R. M., Borthakur, S., Overzier, R., & Leitherer, C. 2015, ApJ, 809, 147, doi: 10.1088/0004-637X/809/2/147

Heckman, T. M., Borthakur, S., Overzier, R., et al. 2011, ApJ, 730, 5, doi: 10.1088/0004-637X/730/1/5

Henry, A., Berg, D. A., Scarlata, C., Verhamme, A., & Erb, D. 2018, ApJ, 855, 96, doi: 10.3847/1538-4357/aab099

Henry, A., Scarlata, C., Martin, C. L., & Erb, D. 2015, ApJ, 809, 19, doi: 10.1088/0004-637X/809/1/19

Herenz, E. C., & Wisotzki, L. 2017, A&A, 602, A111, doi: 10.1051/0004-6361/201629507

Horne, K. 1986, PASP, 98, 609, doi: 10.1086/131801

Inami, H., Bacon, R., Brinchmann, J., et al. 2017, A&A, 608, A2, doi: 10.1051/0004-6361/201731195

Inoue, A. K., Shimizu, I., Iwata, I., & Tanaka, M. 2014, MNRAS, 442, 1805, doi: 10.1093/mnras/stu936

Izotov, Y. I., Guseva, N. G., Fricke, K. J., et al. 2021, A&A, 646, A138, doi: 10.1051/0004-6361/202039772

Izotov, Y. I., Schaerer, D., Thuan, T. X., et al. 2016, MNRAS, 461, 3683, doi: 10.1093/mnras/stw1205

Izotov, Y. I., Worseck, G., Schaerer, D., et al. 2018, MNRAS, 478, 4851, doi: 10.1093/mnras/sty1378

Jaskot, A. E., Dowd, T., Oey, M. S., Scarlata, C., & McKinney, J. 2019, ApJ, 885, 96, doi: 10.3847/1538-4357/ab3d3b

Jaskot, A. E., & Oey, M. S. 2013, ApJ, 766, 91, doi: 10.1088/0004-637X/766/2/91

Jaskot, A. E., Oey, M. S., Scarlata, C., & Dowd, T. 2017, ApJL, 851, L9, doi: 10.3847/2041-8213/aa9d83

Katz, H., Ďurovčíková, D., Kimm, T., et al. 2020, MNRAS, 498, 164, doi: 10.1093/mnras/staa2355

Katz, H., Garel, T., Rosdahl, J., et al. 2022, MNRAS, 515, 4265, doi: 10.1093/mnras/stac1437

Katz, H., Saxena, A., Rosdahl, J., et al. 2023, MNRAS, 518, 270, doi: 10.1093/mnras/stac3019

Kerutt, J., Wisotzki, L., Verhamme, A., et al. 2022, A&A, 659, A183, doi: 10.1051/0004-6361/202141900

Kewley, L. J., & Dopita, M. A. 2002, ApJS, 142, 35, doi: 10.1086/341326

Kulas, K. R., Shapley, A. E., Kollmeier, J. A., et al. 2012, ApJ, 745, 33, doi: 10.1088/0004-637X/745/1/33

Leclercq, F., Bacon, R., Wisotzki, L., et al. 2017, A&A, 608, A8, doi: 10.1051/0004-6361/201731480

Lotz, J. M., Koekemoer, A., Coe, D., et al. 2017, ApJ, 837, 97, doi: 10.3847/1538-4357/837/1/97

Mahler, G., Richard, J., Clément, B., et al. 2018, MNRAS, 473, 663, doi: 10.1093/mnras/stx1971

Malhotra, S., & Rhoads, J. E. 2002, ApJL, 565, L71, doi: 10.1086/338980

Malhotra, S., Rhoads, J. E., Finkelstein, S. L., et al. 2012, ApJL, 750, L36, doi: 10.1088/2041-8205/750/2/L36

Mascia, S., Pentericci, L., Calabro', A., et al. 2023, arXiv e-prints, arXiv:2301.02816, doi: 10.48550/arXiv.2301.02816

Maseda, M. V., Brinchmann, J., Franx, M., et al. 2017, A&A, 608, A4, doi: 10.1051/0004-6361/201730985

Merlin, E., Amorín, R., Castellano, M., et al. 2016, A&A, 590, A30, doi: 10.1051/0004-6361/201527513

Morishita, T., Roberts-Borsani, G., Treu, T., et al. 2022, arXiv e-prints, arXiv:2211.09097, doi: 10.48550/arXiv.2211.09097

Naidu, R. P., Forrest, B., Oesch, P. A., Tran, K.-V. H., & Holden, B. P. 2018, MNRAS, 478, 791, doi: 10.1093/mnras/sty961

Naidu, R. P., Tacchella, S., Mason, C. A., et al. 2020, ApJ, 892, 109, doi: 10.3847/1538-4357/ab7cc9

Nakajima, K., Ellis, R. S., Robertson, B. E., Tang, M., & Stark, D. P. 2020, ApJ, 889, 161, doi: 10.3847/1538-4357/ab6604

Nakajima, K., & Ouchi, M. 2014, MNRAS, 442, 900, doi: 10.1093/mnras/stu902

Nakajima, K., Ouchi, M., Shimasaku, K., et al. 2013, ApJ, 769, 3, doi: 10.1088/0004-637X/769/1/3

—. 2012, ApJ, 745, 12, doi: 10.1088/0004-637X/745/1/12

Neufeld, D. A. 1991, ApJL, 370, L85, doi: 10.1086/185983

Ono, Y., Ouchi, M., Shimasaku, K., et al. 2010, MNRAS, 402, 1580, doi: 10.1111/j.1365-2966.2009.16034.x

Östlin, G., Hayes, M., Duval, F., et al. 2014, ApJ, 797, 11, doi: 10.1088/0004-637X/797/1/11

Pagel, B. E. J., Edmunds, M. G., Blackwell, D. E., Chun, M. S., & Smith, G. 1979, MNRAS, 189, 95, doi: 10.1093/mnras/189.1.95

Pahl, A. J., Shapley, A., Steidel, C. C., Chen, Y., & Reddy, N. A. 2021, MNRAS, 505, 2447, doi: 10.1093/mnras/stab1374

Pengelly, R. M. 1964, MNRAS, 127, 145, doi: 10.1093/mnras/127.2.145

Pentericci, L., Vanzella, E., Castellano, M., et al. 2018, A&A, 619, A147, doi: 10.1051/0004-6361/201732465

Reddy, N. A., Topping, M. W., Shapley, A. E., et al. 2022, ApJ, 926, 31, doi: 10.3847/1538-4357/ac3b4c

Richard, J., Claeyssens, A., Lagattuta, D., et al. 2021, A&A, 646, A83, doi: 10.1051/0004-6361/202039462

Rivera-Thorsen, T. E., Östlin, G., Hayes, M., & Puschnig, J. 2017, ApJ, 837, 29, doi: 10.3847/1538-4357/aa5d0a

Rivera-Thorsen, T. E., Hayes, M., Östlin, G., et al. 2015, ApJ, 805, 14, doi: 10.1088/0004-637X/805/1/14

Robertson, B. E. 2022, ARA&A, 60, 121, doi: 10.1146/annurev-astro-120221-044656

Robertson, B. E., Ellis, R. S., Furlanetto, S. R., & Dunlop, J. S. 2015, ApJL, 802, L19, doi: 10.1088/2041-8205/802/2/L19

Robertson, B. E., Tacchella, S., Johnson, B. D., et al. 2022, arXiv e-prints, arXiv:2212.04480, doi: 10.48550/arXiv.2212.04480

Runnholm, A., Hayes, M., Melinder, J., et al. 2020, ApJ, 892, 48, doi: 10.3847/1538-4357/ab7a91

Sanders, R. L., Shapley, A. E., Topping, M. W., Reddy, N. A., & Brammer, G. B. 2023, arXiv e-prints, arXiv:2301.06696, doi: 10.48550/arXiv.2301.06696

Saxena, A., Robertson, B. E., Bunker, A. J., et al. 2023, arXiv e-prints, arXiv:2302.12805, doi: 10.48550/arXiv.2302.12805

Scarlata, C., Colbert, J., Teplitz, H. I., et al. 2009, ApJL, 704, L98, doi: 10.1088/0004-637X/704/2/L98

Stark, D. P., Ellis, R. S., Chiu, K., Ouchi, M., & Bunker, A. 2010, MNRAS, 408, 1628, doi: 10.1111/j.1365-2966.2010.17227.x

Steidel, C. C., Bogosavljević, M., Shapley, A. E., et al. 2011, ApJ, 736, 160, doi: 10.1088/0004-637X/736/2/160

Tacchella, S., Johnson, B. D., Robertson, B. E., et al. 2022, arXiv e-prints, arXiv:2208.03281, doi: 10.48550/arXiv.2208.03281

Trainor, R. F., Steidel, C. C., Strom, A. L., & Rudie, G. C. 2015, ApJ, 809, 89, doi: 10.1088/0004-637X/809/1/89

Treu, T., Trenti, M., Stiavelli, M., Auger, M. W., & Bradley, L. D. 2012, ApJ, 747, 27, doi: 10.1088/0004-637X/747/1/27

Treu, T., Roberts-Borsani, G., Bradac, M., et al. 2022, ApJ, 935, 110, doi: 10.3847/1538-4357/ac8158

Trump, J. R., Arrabal Haro, P., Simons, R. C., et al. 2023, ApJ, 945, 35, doi: 10.3847/1538-4357/acba8a

Vanzella, E., Calura, F., Meneghetti, M., et al. 2019, MNRAS, 483, 3618, doi: 10.1093/mnras/sty3311

Verhamme, A., Orlitová, I., Schaerer, D., & Hayes, M. 2015, A&A, 578, A7, doi: 10.1051/0004-6361/201423978

Verhamme, A., Orlitová, I., Schaerer, D., et al. 2017, A&A, 597, A13, doi: 10.1051/0004-6361/201629264

Wang, B., Heckman, T. M., Amorín, R., et al. 2021, ApJ, 916, 3, doi: 10.3847/1538-4357/ac0434

Wisotzki, L., Bacon, R., Blaizot, J., et al. 2016, A&A, 587, A98, doi: 10.1051/0004-6361/201527384

Wofford, A., Leitherer, C., & Salzer, J. 2013, ApJ, 765, 118, doi: 10.1088/0004-637X/765/2/118

Xu, X., Henry, A., Heckman, T., et al. 2022, ApJ, 933, 202, doi: 10.3847/1538-4357/ac7225

—. 2023, ApJ, 943, 94, doi: 10.3847/1538-4357/aca89a

Yang, H., Malhotra, S., Rhoads, J. E., & Wang, J. 2017a, ApJ, 847, 38, doi: 10.3847/1538-4357/aa8809

Yang, H., Malhotra, S., Gronke, M., et al. 2017b, ApJ, 844, 171, doi: 10.3847/1538-4357/aa7d4d

Zackrisson, E., Inoue, A. K., & Jensen, H. 2013, ApJ, 777, 39, doi: 10.1088/0004-637X/777/1/39